Solar Energy Materials & Solar Cells 108 (2013) 156–163

Contents lists available at SciVerse ScienceDirect

Solar Energy Materials & Solar Cells

journal homepage: www.elsevier.com/locate/solmat

Solution-processed zinc oxide nanoparticles as interlayer materials for inverted organic solar cells

Mohammed Aziz Ibrahem [a,b,c], Hung-Yu Wei [d], Meng-Hung Tsai [e], Kuo-Chuan Ho [d], Jing-Jong Shyue [b,e], Chih Wie Chu [b,f,*]

[a] Department of Physics, National Taiwan University, Taipei 106, Taiwan
[b] Research Center of Applied Science, Academia Sinica, Taipei 115, Taiwan
[c] Nanoscience and Technology Program, Taiwan International Graduate Program, Academia Sinica, Taipei 115, Taiwan
[d] Institute of Polymer Science and Engineering, National Taiwan University, Taipei 10617, Taiwan
[e] Department of Material Science and Engineering, National Taiwan University, Taipei 106, Taiwan
[f] Department of Photonics, National Chiao Tung University, Hsinchu, 300, Taiwan

ARTICLE INFO

Article history:
Received 28 June 2012
Received in revised form
27 August 2012
Accepted 4 September 2012
Available online 17 October 2012

Keywords:
Polymer solar cells
ZnO
Nanoparticles
Wet grinding
Buffer layer

ABSTRACT

This paper describes inverted bulk heterojunction organic solar cells featuring solution-processed zinc oxide nanoparticles (ZnO NPs) as an electron extraction layer, prepared at relatively low annealing temperatures ($\leq 150\,^{\circ}C$). A solution of ZnO NPs (average size: 25 nm) was prepared using a wet grinding method. When the ZnO interlayer was present in the solar cell, the vertical phase separation of the active layers prepared with and without solvent annealing exhibited similar gradient concentrations and, therefore, similar photocurrent generation, both of which were superior to those of conventional devices incorporating a poly(3,4-ethylenedioxythiophene):poly(styrene sulfonic acid) (PEDOT:PSS) hole extraction layer. We attribute this vertical phase separation to the similar surface energies of the fullerene derivative and the ZnO interlayer. Under simulated air mass (AM) 1.5 G illumination at 100 mW cm^{-2}, the power conversion efficiency of the optimized device was approximately 4%.

1. Introduction

Over the past decades, much effort has been exerted in the quest to improve energy efficiency, to develop renewable energy and clean fuel sources, and to decrease overall greenhouse gas emissions. In particular, the abundance of clean energy from the sun has drawn much attention [1]. Recently, organic solar cells have attracted considerable interest as potential next-generation solar cells because they can be prepared at low cost, with low environmental load and flexibility, and as lightweight alternatives to currently used silicon solar cells [2]. Conducting organic compounds are at the heart of bulk-heterojunction (BHJ) solar cells, which feature an interpenetrating blend of optically active polymers and electron-accepting molecules. The combination of poly(3-hexylthiophene) (P3HT) and [6,6]-phenyl-C_{61}-butyric acid methyl ester (PCBM) in organic blends exhibits particularly promising photovoltaic performance [3]. The traditional BHJ architecture has limited device stability because it features an air-sensitive, low-work-function metal cathode (e.g., calcium), at which oxygen can diffuse into the active layer through pinholes and grain boundaries, leading to its degradation [4]. Furthermore, the traditional BHJ architecture assembles into an undesirable component distribution, with the P3HT-rich region partitioning to the top (air) surface and the PCBM-rich region remaining at the bottom (substrate) surface, as a result of the different surface energies of the photoactive components [5,6]. To improve charge collection, the architecture of BHJ devices can be modified with functional layers inserted at the interfaces between the active layers and the electrodes [7]. Such so-called "inverted" structures can overcomes problems with both the interface instability and the degradation of the indium tin oxide (ITO)-poly(3,4-ethylenedioxythiophene):poly(styrene sulfonic acid) (PEDOT:PSS) interface an inevitability because of the strongly acidic nature of PEDOT:PSS [8]. Further improvements in the performance of the inverted architecture can be expected by reducing the resistivity of the functional buffer layer and optimizing the energy alignment at the acceptor–buffer layer interfaces [9].

Inverted architectures featuring various electron-selective layers, including cesium carbonate (Cs_2O_3) [10], titanium dioxide (TiO_x) [11,12], calcium (Ca) [7], titanium chelate (TIPD) [13], rhenium oxide [14], and ZnO [15–19], have been prepared to

* Corresponding author at: Research Center of Applied Science, Academia Sinica, Taipei 115, Taiwan.
E-mail address: gchu@gate.sinica.edu.tw (C.W. Chu).

0927-0248/$ - see front matter © 2012 Elsevier B.V. All rights reserved.
http://dx.doi.org/10.1016/j.solmat.2012.09.007

improve electron transport and extraction. Applying the same interlayer concept to the opposite electrode, several transition metal oxides, including vanadium oxide (V_2O_5) [20–22] and molybdenum oxide (MoO_3) [23,24], have been exploited as interfacial hole extraction layers between the positive electrode and the photoactive layer in organic photovoltaic (OPVs). Among the transition metal oxides, ZnO is a promising candidate because of its relatively high electron mobility, environmental stability, and optical transmittance in the visible range [25], its wide and direct band gap (3.37 eV), and its large exciton binding energy (60 meV) [26]. Moreover, thin films of ZnO are readily prepared through deposition using solution processing and subsequent thermal annealing treatment.

Although many fabrication methods can be employed to prepare ZnO nanoparticles (NPs), including sol–gel processes [11,27,28], vapor phase synthesis [29], simple solution combusting [26], and spray pyrolysis [30], these methods generally require complex equipment and complicated operational procedures; therefore, the challenge remains to develop simple routes for the synthesis of metal oxide NPs in high yield. In this paper, we report a wet grinding method for the preparation of ZnO NPs, using ethylene glycol (EG) as the solvent. Unlike the approaches mentioned above, this solution-based method is relatively simple and convenient; very cheap and facile; environmentally friendly; and provides the resulting NP solutions in a pure and well-dispersed form (stable for hundreds of hours without precipitation) without the need for surfactants. These clean NP solutions are processable through spin coating at low temperature (150 °C) to form high-quality, continuous films free from cracks and pinholes. In addition, layers of P3HT:PCBM deposited through spin-coating on top of ZnO interlayers prepared with and without solvent annealing exhibit similar phase separation morphologies determined from X-ray photoelectron spectroscopy (XPS) depth profiles of the concentration gradients of the donor and acceptor moieties in the vertical direction while maintaining very smooth surfaces. Notably, the performance of inverted-structure devices featuring ZnO interfacial layers prepared with or without solvent annealing was better than that of conventional devices featuring a PEDOT:PSS buffer layer.

2. Experimental methods

2.1. ZnO NPs and thin film preparation

Different types of surfactant have been used to stabilize ZnO NPs prepared using various methods. Huang et al. stabilized ZnO NPs in EG solvent by adding a silane coupling agent [31]; Ni et al. synthesized ZnO NPs using a simple solution-combusting method employing a mixture of EtOH and EG as starting solvents [26]; and Krebs stabilized ZnO NP ink with methoxyethoxyacetic acid (MEA) in WS-1 solvent and chlorobenzene with *o*-xylene and WS-1 [32]. In this study, ZnO powder (UniRegion Bio-Tech) was dispersed in pure EG (J.T. Baker) at a concentration of 5 wt%, without any surfactant or modification, for use as the starting material for grinding. High-energy ball milling was performed at room temperature using a batch-type grinder (JBM-B035) operated at a rate of 2000 rpm. The milling duration was typically in the range 60–420 min. The resultant solution could be diluted to a lower concentration without any precipitation. Prior to spin-coating with thin ZnO films, ITO-coated glass substrates ($<10\ \Omega\ sq^{-1}$, RiTdisplay) were cleaned through ultrasonication in detergent-containing water and twice with deionized (DI) water (15 min each), dried in an oven, and then treated with ultraviolet (UV)/ozone for 15 min. The ZnO NP solution was coated on top of the ITO glass through spin-coating at 4000 rpm for 60 s and then thermally annealed at 150 °C for 60 min, providing a thin film having a thickness of approximately 40 nm.

2.2. ZnO thin film characterization

The average particle size was measured using a particle size analyzer (Brookhaven 90 plus Sn11408). The absorption and transmittance spectra of the ZnO thin films were recorded using a Jasco V-670 UV–vis–NIR spectrophotometer. The surface morphologies of the thin films were measured through scanning electron microscopy (SEM; FEI Nova200) and atomic force microscopy (AFM; Veeco di Innova). The thickness of the thin film was measured using a Veeco Dektak 150 alpha step surface profiler. The valence band maximum (VBM) of the ZnO film was measured using ultraviolet photoelectron spectroscopy (UPS; PHI 5000 Versa Probe scanning ESCA microprobe); the band gap (E_g) was obtained from the UV absorption edge. Contact angles and surface energies were measured using a Slideaway instrument.

2.3. PSC fabrication and characterization

Devices featuring a ZnO interfacial layer in an inverted structure (ITO/ZnO/P3HT:PCBM/V_2O_5/AL; displayed in Fig. 1 along with a basic energy level diagram of the component materials) were fabricated using different mechanisms for solidification of the active layer. Device A was prepared with "slow-growth" deposition of the active layer, spin-coated from a solution containing P3HT:PCBM (1:1, w/w) in 1,2-dichlorobenzene on top of the ZnO film, and then it was dried

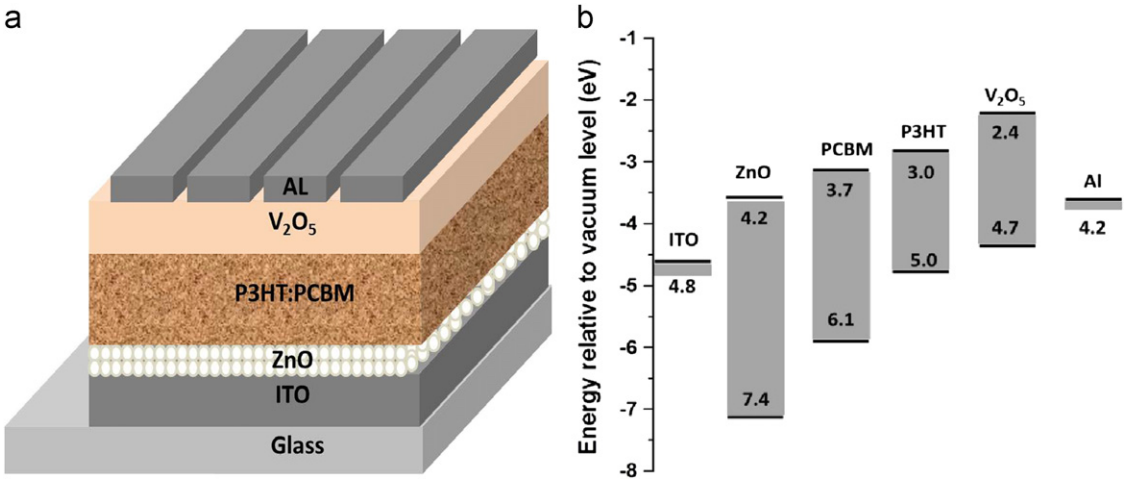

Fig. 1. (a) Device structure. (b) Energy level diagram of the component materials used for device fabrication.

for 30 min in a covered Petri glass dish for solvent evaporation; subsequently, the films were annealed at 130 °C for 30 min. Device B, featuring the "fast-grown" active layer, was directly thermally annealed at 130 °C for 30 min without solvent evaporation. The active layer of device C was prepared without solvent or thermal annealing, while the active layer of device D was prepared as in the case of device A, but on the ITO surface (i.e., without a ZnO interlayer). For the regular device E (ITO/PEDOT:PSS/P3HT:PCBM/V_2O_5/AL), the active layer was prepared in manner similar to that of device A. The thickness of the active layer in each device was approximately 200 nm. Layers of V_2O_5 (99.6% Alfa Aesar; 10 nm) and Al (100 nm) were sequentially thermally evaporated through a shadow mask under vacuum (pressure: $<6\times10^{-6}$ Torr). The active area of each device was 10 mm^2; its performance was tested inside a glove box under simulated AM 1.5 G irradiation conditions (100 mW cm^{-2}) using a Xenon (Xe) lamp-based solar simulator (Thermal Oriel1000W). The external incident photon-to-current efficiency (IPCE) spectra were recorded under short-circuit conditions. The devices were encapsulated in UV gel and transparent glass before they were removed from the glove box. The light source was a 450 W Xe lamp (Oriel Instruments, Model 6123NS). The light output from the monochromator (Oriel Instruments, Model 74100) was focused on the photovoltaic cell being tested.

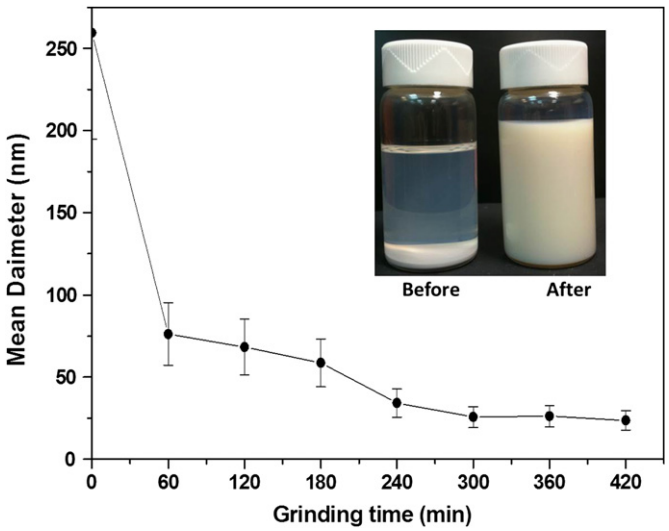

Fig. 2. Particle sizes in ZnO powders obtained after different grinding times. Inset: Sedimentation from ZnO solutions before and after grinding for 420 min.

3. Results and discussion

The ZnO NPs exhibited size-dependent dissolution behavior, with the smallest ZnO NPs exhibiting the greatest tendency for

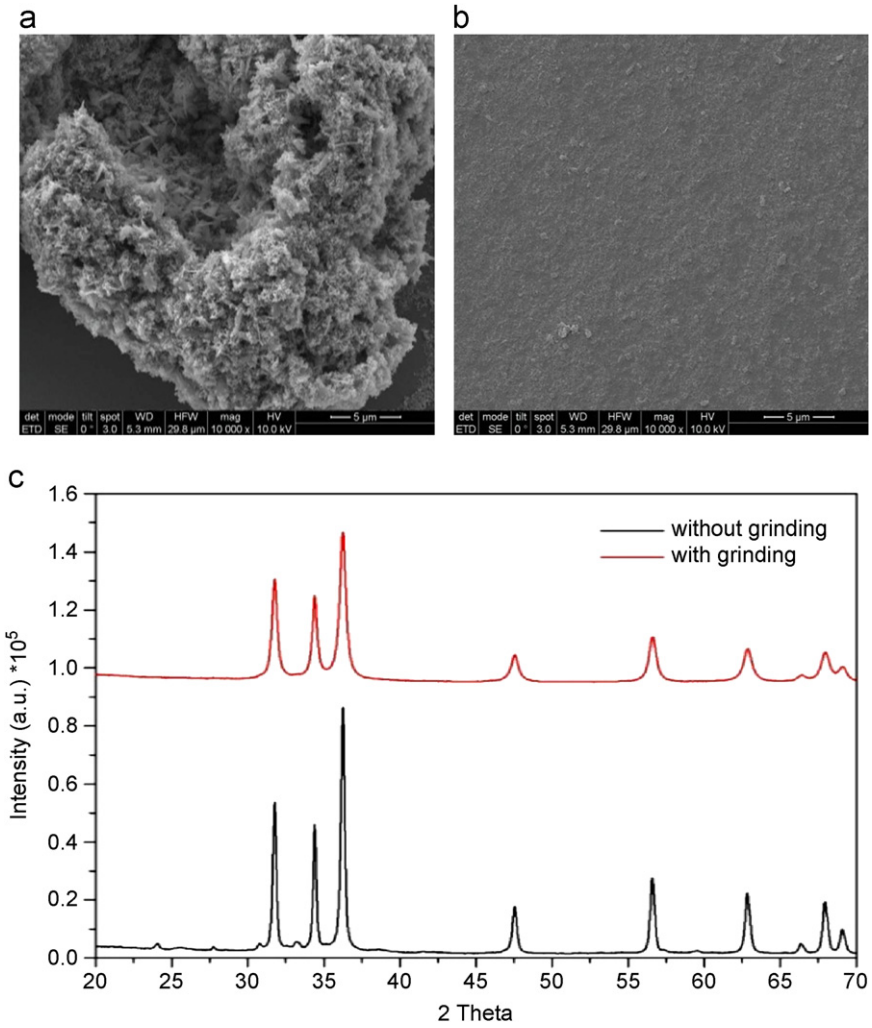

Fig. 3. (a) and (b) SEM images of thin films formed through spin-coating (4000 rpm) and annealing (150 °C, 60 min) of (a) the non-ground powder and (b) the ground 3 wt% ZnO solution. (c) Corresponding XRD patterns of ZnO powders prepared with and without grinding for 420 min.

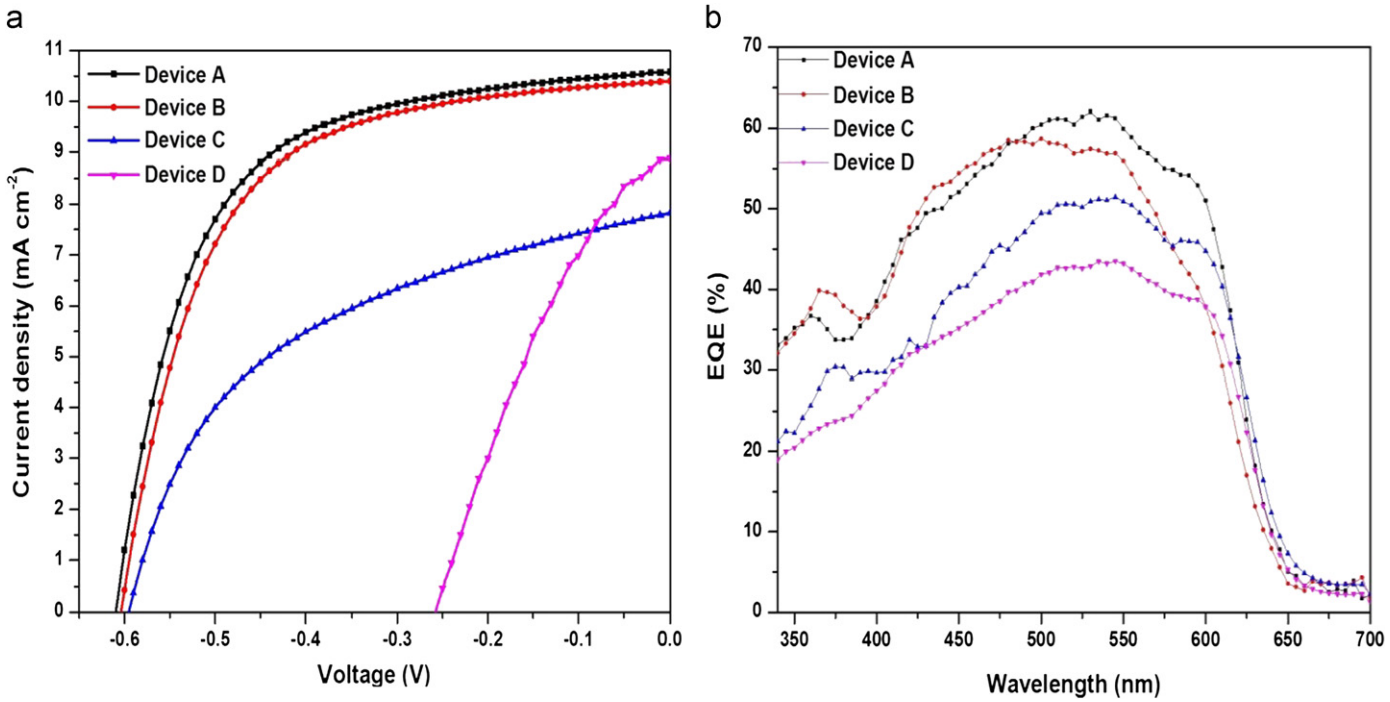

Fig. 4. (a) *J–V* characteristics and (b) IPCE spectra of the inverted solar cell devices A ("fast growth"), B ("slow growth" of active layer), C (fast grown without thermal annealing), and D (without ZnO layer).

dispersion, while the aggregated NPs displayed decreased propensity for dispersion, attributable to differences in surface tension, which is size- and shape-dependent [33,34]. To obtain much smaller, more uniformly shaped, and better-dispersed NPs, longer grinding times were required. The particle size decreased upon increasing the grinding time, with the initially non-uniform particles (>250 nm) reaching approximately 25 nm after 420 min of grinding (Fig. 2). We performed sedimentation tests by storing ZnO solutions (prepared with and without grinding) in EG for more than six months. The ZnO NPs prepared without grinding precipitated completely after a few hours, but the ZnO NPs prepared with grinding were highly stable without any precipitation (see inset to Fig. 2). Thus, the grinding process increased the compatibility between the ZnO NPs and the organic solvent, increased the repulsive forces among the particles, and prevented the ZnO NPs from aggregating. We obtained a discontinuous film with very large grains (5 μm) from the non-ground ZnO solution (Fig. 3a); in contrast, a uniform continuous film without pinholes or cracks was formed from the ground ZnO NP solution (Fig. 3b). Thus, the uniform and smaller particles formed more-compact and denser films, without pinholes or cracks, thereby presumably decreasing the potential barrier and, accordingly, increasing the degree of electron extraction from the interface with the polymer blend film. The X-ray diffraction (XRD) patterns in Fig. 3(c) reveal the stoichiometries of the ZnO powders prepared with and without grinding. The nearly identical values of 2θ the XRD peaks imply the same crystallinity, with the decreased intensity and broadening of the peaks after grinding being consistent with decreased grain and lattice sizes.

Thermal and solvent annealing are currently the most popular methods for controlling the morphologies of polymeric active layers, particularly to increase a material's crystallinity and to develop suitably phase-separated domains for efficient carrier transport. It was not until 2005 that the combination of thermal and solvent annealing was demonstrated to significantly enhance PSC efficiency [35]. Rapid solidification of the BHJ generally produces devices exhibiting poor power conversion efficiencies

Table 1
Device performance parameters of inverted P3HT:PCBM solar cells fabricated with a ZnO film as the electron extraction layer.

Device	V_{oc} (volt)	J_{sc} (mA cm^{-2})	FF (%)	PCE (%)	
				Best	Average[a]
A	0.61 ± 0.012	10.65 ± 0.23	61.26 ± 0.5	3.98	3.74
B	0.6 ± 0.011	10.4 ± 0.2	61.22 ± 0.6	3.8	3.58
C	0.59 ± 0.023	7.79 ± 0.4	48.15 ± 0.8	2.2	2.04
D	0.25 ± 0.027	8.66 ± 0.5	37 ± 0.67	0.8	0.72
E	0.6 ± 0.015	9.24 ± 0.18	65.8 ± 0.5	3.65	3.5

[a] PCEs were averaged over 12 solar cells.

(PCEs). The challenge remains to develop simple methods, without the need for solvent annealing, to obtain high efficiencies. In this study, we observed comparable PCEs both with and without solvent annealing when using the ZnO NPs as interlayer films in the inverted device structure. Fig. 4(a) displays the current density–voltage (*J–V*) characteristics of the devices; Table 1 summarizes their extracted device parameters. The variations in device performance were not significant in terms of open-circuit voltage (V_{oc}), short-current density (J_{sc}), or fill factor (FF)between device A ("slow grown"; PCE=3.98%) and device B ("fast grown without solvent annealing"; PCE=3.8%); these comparable performance parameters resulted from vertical phase segregation of the P3HT:PCBM blend film after insertion of ZnO as an electron extraction layer. In contrast, device C ("fast grown without solvent and thermal annealing"; PCE=2.2%) and the conventional device E ("slow grown" with PEDOT:PSS buffer layer; PCE=3.65%) exhibited comparable values of V_{oc}, but lower values of J_{sc} and FF, relative to devices A and B. Because device C, with and without solvent annealing of the active layer given a similar performances PCE < 2.2%, annealing of the active layer (at 130 °C for 30 min) enhanced the phase separation and crystallinity of the P3HT chains, leading to significant improvement in the values of J_{sc} and FF and, therefore, the device performance. Device D ("slow grown without ZnO interlayer"; PCE=0.8%) exhibited tremendous

decreases in V_{oc}, FF, and performance, revealing the important role that the ZnO interlayer played in the device performance. The IPCE spectra in Fig. 4(b) reveal that the maximum IPCE (63%) was that for device A, indicative of efficient photon-to-electron conversion with a higher value of J_{sc}. The improvement in short-circuit current density is consistent with the greater incident photon-to-current conversion efficiency, and of a device featuring a more highly transparent ZnO film near the absorption spectrum of P3HT:PCBM providing a higher photocurrent. A sharp drop in IPCE at wavelengths below 400 nm is clearly evident, with small increases in the UV region, for all devices incorporating a ZnO layer, due to the strong absorption of the film near the band edge of ZnO. This observation suggests that the blend layer morphologies and charge carrier percolation networks were affected by the choice of processing method [36]. The advantages of vertical segregation and of the inverted structure over the regular structure are apparent under the same spin-coating parameters.

It is believed that the surface morphology of a ZnO film, in term of its wettability and adhesion with the polymer layer, will affect the performance of the corresponding device. Small contact angles generally indicate hydrophilic properties, with good wetting and adhesion [37]. Therefore, we measured surface morphologies, roughnesses, and contact angles to investigate the surface qualities of our ZnO films at the blend interface (with and without solvent annealing). In a fluid medium, P3HT molecules will move toward the relatively hydrophobic side, causing the top surface air-blend interface region to be P3HT-rich and the bottom surface ITO-blend interface region to be PCBM-rich [38]. Table 2 summarizes the average surface energies and contact angles of blend films featuring a ZnO interlayer and pure P3HT and PCBM layers. The surface energy of the ZnO film was higher than those of the pure P3HT layer and of the reference blend film without a ZnO layer, but it was similar to that of the pure PCBM layer. The surface energies of the blend films featuring ZnO layers grown with and without solvent annealing were similar, and they were closer to that of pure P3HT than they were to that of PCBM. Based on contact angle measurements, we conclude that the ZnO interlayer induced the diffusion of PCBM toward the bottom surface, rather than to the top surface, with either mechanism for growing the blend film, producing similar degrees of vertical phase separation.

Table 2
Surface energies and contact angles of ZnO thin films and the components of the active layer blend.

Film	H_2O contact angle (degree)	EG contact angle (degree)	Surface energy (mN cm^{-2})
ZnO	86.1	55	38.24
Pure PCBM	73.05	60.3	37.87
Pure P3HT	95.87	70.1	25.53
P3HT:PCBM	96.7	87.4	30.43
ZnO+P3HT:PCBM slow growth	87.88	78.75	26.32
ZnO+P3HT:PCBM fast growth	90.92	79.65	26.95

To further investigate the vertical phase separation, we measured the depth profiles of the blend P3HT:PCBM active layer on top of the ZnO/ITO surface (Fig. 5). Here, sulfur (S) atoms represent the relative amount of P3HT within the photoactive layer, zinc (Zn) atoms represent ZnO, and indium (In) atoms represent ITO. The vertical gradients of P3HT in the blend films with and without solvent annealing exhibited similar behavior, with the concentration distribution (P3HT-rich on the surface; PCBM-rich near the ZnO adjacent to the cathode) indicating vertical segregation on the ZnO-coated ITO side. A small difference appeared, however, in the gradients of the two curves, namely of the P3HT gradients in the blend films prepared using the two growing methods. The atomic concentration of S atoms in the case of the slowly grown film was lower than that of the rapidly grown film, indicating a higher concentration of PCBM; in contrast, the P3HT:PCBM blend film prepared without a ZnO interlayer did not reveal such a clear concentration gradient. We conclude that a slow rate of solvent evaporation facilitates the growth of highly crystalline P3HT; under such conditions, a portion of the PCBM molecules, with a faster rate of crystallization than that of the polymer, were gradually expelled from the P3HT domains, resulting in the formation of P3HT- and PCBM-rich domains. These results are consistent with the surface energies and contact angles listed in Table 2. Because P3HT is a hole-conducting p-type semiconductor and PCBM is an electron-

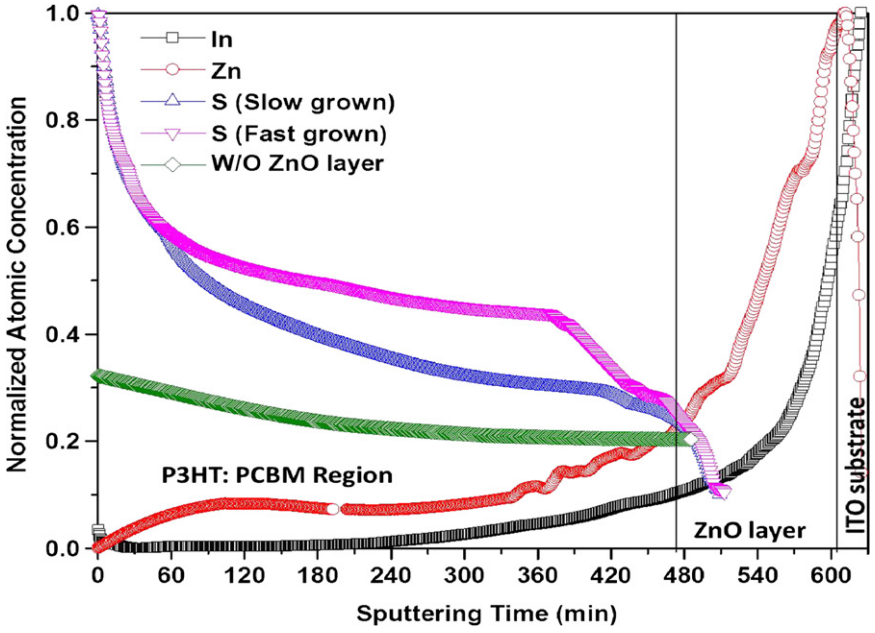

Fig. 5. Depth profiles of In, Zn, and *S* atoms (representing ITO, ZnO, and P3HT, respectively) in the P3HT:PCBM blend films of inverted-structure BHJ solar cells.

conducting n-type semiconductor, this vertical inhomogeneous distribution is more congruous in the inverted device structure than in the regular one.

We further investigated the effect of the inserted ZnO interlayer on the device performance as well as the morphology by varying concentration of the ZnO solution from 1 to 5 wt%. Fig. 6(a) displays the *J–V* characteristics of inverted devices prepared with different concentrations of ZnO in the films. The highest PCE (3.98%) was that obtained from the 3 wt% solution, with values of J_{sc}, V_{oc}, and FF of 10.65 mA cm^{-2}, 0.61 V, and 61.26%, respectively; the other concentrations provided lower device performance parameters. We believe that this behavior is related to the transparency of the 3 wt% film near the absorption spectrum of P3HT:PCBM being higher than those of the films prepared at the other concentrations (Fig. 6b). The transparency of the films changed as a result of variations in film morphology

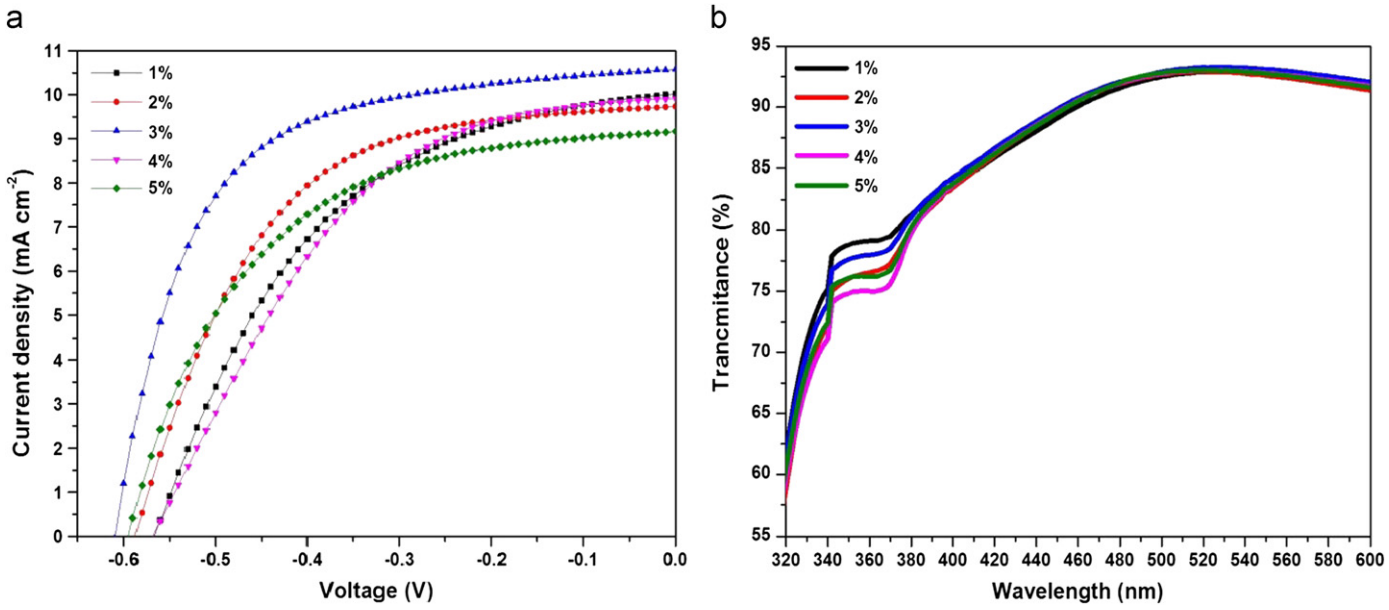

Fig. 6. (a) *J–V* characteristics and (b) transmittance spectra of inverted-structure solar cells incorporating ZnO films prepared through spin-coating (4000 rpm) of ZnO NP solutions of various concentrations and subsequent annealing (150 °C, 60 min).

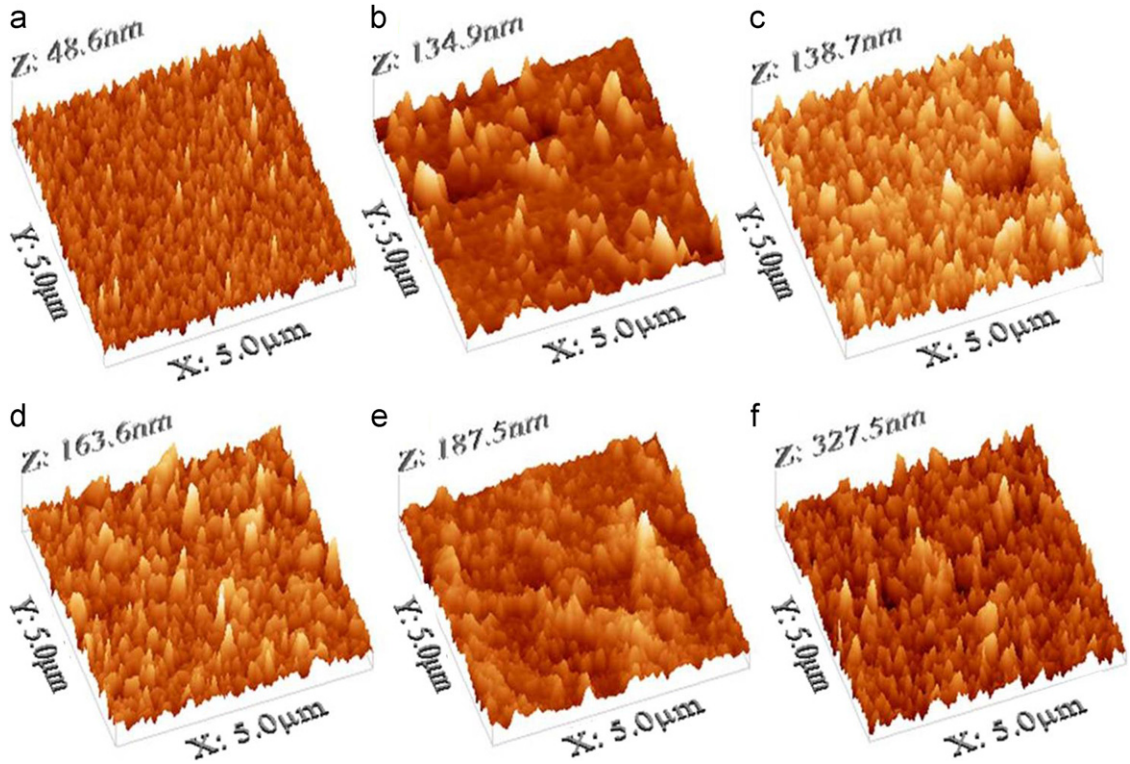

Fig. 7. Tapping-mode AFM topographic images of (a) bare ITO and (b–f) ZnO films prepared through spin-coating (4000 rpm) onto ITO glass from ZnO NP solutions of various concentrations [(b) 1, (c) 2, (d) 3, (e) 4, and (f) 5 wt%] and subsequent thermal annealing (150 °C, 60 min).

when prepared at the different concentrations. To investigate the changes in morphology and surface roughness, we recorded AFM images of the ZnO films deposited from solutions at different concentrations. Fig. 7 reveals that the grain size increased upon increasing the concentration of the ZnO solution, presumably because a greater amount of solute increased the probability of solute clustering to form larger grains. The grain sizes revealed in SEM images (not shown) were consistent with the measured surface roughnesses, with larger grain sizes resulting in rougher films. The surface roughnesses (root-mean-square values) of the films prepared from ZnO NP solutions at concentrations of 1, 2, 3, 4, and 5 wt% were 10.02, 10.93, 12.33, 14.23, and 15.48 nm, respectively. These small variations in surface roughness and grain size of the ZnO films cannot be correlated with the variations in device performance, suggesting that the vertical phase separation in the blend film was maintained because the surface properties remained unchanged. We conclude that the concentration of ZnO solutes in the film should be controlled to maximize PCE.

4. Conclusion

We have successfully synthesized ZnO NPs through a simple, cheap, and clean wet-grinding method. Corresponding solution-processed ZnO interlayers effectively block holes and collect electrons from PCBM. This fabrication approach requires no vacuum processing, a relatively low annealing temperature (150 °C), and removes the need for PEDOT:PSS. Furthermore, the degree of vertical phase separation in the rapidly grown active layer was independent of the surface morphology of the ZnO layer and provided a device with efficiency comparable to that of slow growth, thereby decreasing the fabrication time and the cost of the resulting solar cell. Thus, our method for preparing NPs is a very promising one that might contribute to decreasing the cost of PV technologies.

Acknowledgment

We thank Tian-wey Lan and Professor Yuan-Yang Chen of the Institute of Physics at Academia Sinica for the XRD measurements. Dr. Chu thanks the National Science Council (NSC), Taiwan (NSC100-2221-E-001–009), and the Thematic Project of Academia Sinica, Taiwan (AS-100-TP-A05), for financial support.

References

[1] X. Yang, X. Su, M. Shen, F. Zheng, Y. Xin, L. Zhang, M. Hua, Y. Chen, V.G. Harris, Enhancement of photocurrent in ferroelectric films via the incorporation of narrow bandgap nanoparticles, Advanced Materials 24 (2012) 1202–1208.
[2] T. Kuwabara, C. Iwata, T. Yamaguchi, K. Takahashi, Mechanistic insights into UV-induced electron transfer from PCBM to titanium oxide in inverted-type organic thin film solar cells using AC impedance spectroscopy, ACS Applied Materials and Interfaces 2 (2010) 2254–2260.
[3] P.P. Boix, J. Ajuria, R. Pacios, G. Garcia-Belmonte, Carrier recombination losses in inverted polymer: fullerene solar cells with ZnO hole-blocking layer from transient photovoltage and impedance spectroscopy techniques, Journal of Applied Physics 109 (2011) 074514-1–074514-5.
[4] A.K.K. Kyaw, X.W. Sun, C.Y. Jiang, G.Q. Lo, D.W. Zhao, D.L. Kwong, An inverted organic solar cell employing a sol–gel derived ZnO electron selective layer and thermal evaporated MoO[sub 3] hole selective layer, Applied Physics Letters 93 (2008) 221107-1–221107-3.
[5] M. Campoy-Quiles, T. Ferenczi, T. Agostinelli, P.G. Etchegoin, Y. Kim, T.D. Anthopoulos, P.N. Stavrinou, D.D. Bradley, J. Nelson, Morphology evolution via self-organization and lateral and vertical diffusion in polymer:fullerene solar cell blends, Nature Materials 7 (2008) 158–164.
[6] Z. Xu, L.-M. Chen, G. Yang, C.-H. Huang, J. Hou, Y. Wu, G. Li, C.-S. Hsu, Y. Yang, Vertical phase separation in poly(3-hexylthiophene): fullerene derivative blends and its advantage for inverted structure solar cells, Advanced Functional Materials 19 (2009) 1227–1234.
[7] D.W. Zhao, S.T. Tan, L. Ke, P. Liu, A.K.K. Kyaw, X.W. Sun, G.Q. Lo, D.L. Kwong, Optimization of an inverted organic solar cell, Solar Energy Materials and Solar Cells 94 (2010) 985–991.
[8] K. Aung Ko Ko, S. Xiaowei, Z. De Wei, T. Swee Tiam, Y. Divayana, H.V. Demir, Improved inverted organic solar cells with a sol–gel derived indium-doped zinc oxide buffer layer, IEEE Journal of Selected Topics in Quantum Electronics 16 (2010) 1700–1706.
[9] T. Stubhan, H. Oh, L. Pinna, J. Krantz, I. Litzov, C.J. Brabec, Inverted organic solar cells using a solution processed aluminum-doped zinc oxide buffer layer, Organic Electronics 12 (2011) 1539–1543.
[10] L. Yang, H. Xu, H. Tian, S. Yin, F. Zhang, Effect of cathode buffer layer on the stability of polymer bulk heterojunction solar cells, Solar Energy Materials and Solar Cells 94 (2010) 1831–1834.
[11] H. Oh, J. Krantz, I. Litzov, T. Stubhan, L. Pinna, C.J. Brabec, Comparison of various sol–gel derived metal oxide layers for inverted organic solar cells, Solar Energy Materials and Solar Cells 95 (2011) 2194–2199.
[12] J.-H. Huang, H.-Y. Wei, K.-C. Huang, C.-L. Chen, R.-R. Wang, F.-C. Chen, K.-C. Ho, C.-W. Chu, Using a low temperature crystallization process to prepare anatase TiO_2 buffer layers for air-stable inverted polymer solar cells, Energy and Environmental Science 3 (2010) 654–658.
[13] Z. Tan, W. Zhang, Z. Zhang, D. Qian, Y. Huang, J. Hou, Y. Li, High-performance inverted polymer solar cells with solution-processed titanium chelate as electron-collecting layer on ITO electrode, Advanced Materials 24 (2012) 1476–1481.
[14] H. Xu, L.-y. Yang, H. Tian, S.-g. Yin, F. Zhang, Rhenium oxide as the interfacial buffer layer for polymer photovoltaic cells, Optoelectronics Letters 6 (2010) 176–178.
[15] Y. Sun, J.H. Seo, C.J. Takacs, J. Seifter, A.J. Heeger, Inverted polymer solar cells integrated with a low-temperature-annealed sol–gel-derived ZnO Film as an electron transport layer, Advanced Materials 23 (2011) 1679–1683.
[16] P.P. Boix, J. Ajuria, I. Etxebarria, R. Pacios, G. Garcia-Belmonte, J. Bisquert, Role of ZnO electron-selective layers in regular and inverted bulk heterojunction solar cells, ournal of Physical Chemistry Letters 2 (2011) 407–411.
[17] T. Yang, W. Cai, D. Qin, E. Wang, L. Lan, X. Gong, J. Peng, Y. Cao, Solution-processed zinc oxide thin film as a buffer layer for polymer solar cells with an inverted device structure, Journal of Physical Chemistry C 114 (2010) 6849–6853.
[18] F.C. Krebs, M. Jørgensen, K. Norrman, O. Hagemann, J. Alstrup, T.D. Nielsen, J. Fyenbo, K. Larsen, J. Kristensen, A complete process for production of flexible large area polymer solar cells entirely using screen printing—first public demonstration, Solar Energy Materials and Solar Cells 93 (2009) 422–441.
[19] F.C. Krebs, Y. Thomann, R. Thomann, J.W. Andreasen, A simple nanostructured polymer/ZnO hybrid solar cell-preparation and operation in air, Nanotechnology 19 (2008) 424013-1–424013-12.
[20] K. Zilberberg, S. Trost, H. Schmidt, T. Riedl, Solution processed vanadium pentoxide as charge extraction layer for organic solar cells, Advanced Energy Materials 1 (2011) 377–381.
[21] I. Hancox, L.A. Rochford, D. Clare, P. Sullivan, T.S. Jones, Utilizing n-type vanadium oxide films as hole-extracting layers for small molecule organic photovoltaics, Applied Physics Letters 99 (2011) 013304-1–013304-3.
[22] N. Espinosa, H.F. Dam, D.M. Tanenbaum, J.W. Andreasen, M. Jørgensen, F.C. Krebs, Roll-to-roll processing of inverted polymer solar cells using hydrated vanadium(V)oxide as a PEDOT:PSS replacement, Materials 4 (2011) 169–182.
[23] T. Yang, M. Wang, Y. Cao, F. Huang, L. Huang, J. Peng, X. Gong, S.Z.D. Cheng, Y. Cao, Polymer solar cells with a low-temperature-annealed sol–gel-derived MoOx film as a hole extraction layer, Advanced Energy Materials 2 (2012) 523–527.
[24] J.-H. Huang, T.-Y. Huang, H.-Y. Wei, K.-C. Ho, C.-W. Chu, Wet-milled transition metal oxide nanoparticles as buffer layers for bulk heterojunction solar cells, RSC Advances 2 (2012) 7487–7491.
[25] H. Cheun, C. Fuentes-Hernandez, Y. Zhou, W.J. Potscavage, S.-J. Kim, J. Shim, A. Dindar, B. Kippelen, Electrical and optical properties of ZnO processed by atomic layer deposition in inverted polymer solar cells, The Journal of Physical Chemistry C 114 (2010) 20713–20718.
[26] Y. Ni, X. Cao, G. Wu, G. Hu, Z. Yang, X. Wei, Preparation, characterization and property study of zinc oxide nanoparticles via a simple solution-combusting method, Nanotechnology 18 (2007) 155603-1–155603-6.
[27] Z. Liang, Q. Zhang, O. Wiranwetchayan, J. Xi, Z. Yang, K. Park, C. Li, G. Cao, Effects of the morphology of a ZnO buffer layer on the photovoltaic performance of inverted polymer solar cells, Advanced Functional Materials 22 (2012) 2194–2201.
[28] S. Sanchez, S. Berson, S. Guillerez, C. Lévy-Clément, V. Ivanova, Toward high-stability inverted polymer solar cells with an electrodeposited ZnO electron transporting layer, Advanced Energy Materials 2 (2012) 541–545.
[29] C.-Y. Lee, Y.-T. Haung, W.-F. Su, C.-F. Lin, Electroluminescence from ZnO nanoparticles/organic nanocomposites, Applied Physics Letters 89 (2006) 231116-1–231116-3.
[30] N.O.V. Plank, M.E. Welland, J.L. MacManus-Driscoll, L. Schmidt-Mende, The backing layer dependence of open circuit voltage in ZnO/polymer composite solar cells, Thin Solid Films 516 (2008) 7218–7222.
[31] H.C. Huang, T.E. Hsieh, Highly stable precursor solution containing ZnO nanoparticles for the preparation of ZnO thin film transistors, Nanotechnology 21 (2010) 295707-1–295707-7.
[32] F.C. Krebs, Polymer solar cell modules prepared using roll-to-roll methods: knife-over-edge coating, slot-die coating and screen printing, Solar Energy Materials and Solar Cells 93 (2009) 465–475.

[33] S.W. Bian, I.A. Mudunkotuwa, T. Rupasinghe, V.H. Grassian, Aggregation and dissolution of 4 nm ZnO nanoparticles in aqueous environments: influence of pH, ionic strength, size, and adsorption of humic acid, Langmuir: The ACS Journal of Surfaces and Colloids 27 (2011) 6059–6068.
[34] J. Huang, C. Yang, Z. Ho, D. Kekuda, M. Wu, F. Chien, P. Chen, C. Chu, K. Ho, Annealing effect of polymer bulk heterojunction solar cells based on polyfluorene and fullerene blend, Organic Electronics 10 (2009) 27–33.
[35] G. Li, R. Zhu, Y. Yang, Polymer solar cells, Nature Photonics 6 (2012) 153–161.
[36] J.-H. Chang, Y.-H. Chen, H.-W. Lin, Y.-T. Lin, H.-F. Meng, E.-C. Chen, Highly efficient inverted rapid-drying blade-coated organic solar cells, Organic Electronics 13 (2012) 705–709.
[37] Y.C. Jung, B. Bhushan, Contact angle, adhesion and friction properties of micro-and nanopatterned polymers for superhydrophobicity, Nanotechnology 17 (2006) 4970–4980.
[38] H.-H. Liao, L.-M. Chen, Z. Xu, G. Li, Y. Yang, Highly efficient inverted polymer solar cell by low temperature annealing of Cs[sub 2]CO[sub 3] interlayer, Applied Physics Letters 92 (2008) 173303-1–173303-3.